

CCD $UBV(RI)_{KC}$ photometry and dynamics of the open cluster NGC 1513

İnci Akkaya Oralhan¹, Hikmet Çakmak², Yüksel Karataş^{3*}, Raúl Michel⁴, and Charles Bonatto⁵

¹Department of Astronomy and Space Sciences, Faculty of Arts and Sciences, Erciyes University, Talas Yolu, 38039, Kayseri, Türkiye

²Department of Computer Sciences, Science Faculty, İstanbul University, 34134, Vezneciler-Istanbul, Türkiye

³Department of Astronomy and Space Sciences, Science Faculty, İstanbul University, 34116, Üniversite-Istanbul, Türkiye

⁴Observatorio Astronómico Nacional, Universidad Nacional Autónoma de México, Apartado Postal 877, C.P. 22800, Ensenada, B.C., México

⁵Universidade Federal do Rio Grande do Sul, Departamento de Astronomia, CP 15051, RS, Porto Alegre 91501-970, Brazil

Accepted XXX. Received YYY; in original form ZZZ

ABSTRACT

We derive astrophysical parameters of the open cluster NGC 1513 by means of colour indices built with new CCD $UBV(RI)_{KC}$ photometry. Based on early-type members, the mean foreground reddening and total to selective extinction ratio are $E(B-V)=0.79\pm 0.09$ mag and $R_V=2.85\pm 0.05$. Through the differential grid method, we derive the metal abundance $[Fe/H]=-0.06$ dex ($Z=+0.013$), which is consistent with the value $[Fe/H]=-0.088$ of the bright giant member-LAMOST – 695710060. The $Z=+0.013$ isochrone fit to the $V \times (B-V)$ colour-magnitude diagram leads to a turn-off age of 224 ± 27 Myr (thus an intermediate-age cluster), and a distance modulus of $(V_0-M_V)=10.90\pm 0.15$ mag, thus implying a distance from the Sun $d=1514\pm 105$ pc. Within the uncertainties, our photometric distance is consistent with the value $d=1435\pm 14$ pc from the Gaia DR3 parallax. We find signs of small mass segregation through a minimum spanning tree analysis for the 190 most massive stars, together with the rather steep mass function ($\chi = +2.39$) slope. The high core to half-light radius ratio $R_{core}/R_h = 0.82$, together with the compact half-light to tidal radius ratio $R_h/R_t = 0.22$, suggest that it is probably related to cluster-formation effects, due to little dynamical evolution, instead of driving its dynamical evolution by internal relaxation. Indeed, NGC 1513 is located in the second quadrant ($\ell = 152^\circ.59$ and Galactocentric distance $R_{GC} = 9.57$ kpc), which tends to minimize tidal effects by external processes and tidal disruption. Therefore, internal mass segregation effects in NGC 1513 seem to be more efficient than cluster evaporation processes. We find that NGC 1513 migrated about 0.50 kpc from its birth place.

Key words: (Galaxy:) open clusters and associations:general - Galaxy: abundances - Galaxy: evolution

1 INTRODUCTION

U magnitudes are of importance for deriving the reddenings, photometric metal abundances, and also ages of the open clusters (OCs). The errors of U -magnitudes increase towards fainter magnitudes. The errors of σ_{U-B} are always larger, due to the smaller sensitivity of the CCD in the ultraviolet. Most CCDs which have low UV response often produce an effective wavelength too far to the red when the same photoelectric filters were used (Sung and Bessell 2000). The so-called red leak in the used U filter also worsens the situation. As emphasized by Bessell (2005), owing to large differences in U filter between CCDs, achieving of a good match is difficult. The U and B filters with Landolt system do not provide good match to the Johnson system as those used by Cousins, thus cause some systematic differences in some colour indices between the Landolt and Cousins $UBVRI$ systems (Landolt 1973, 1983). These potential effects cause a scattered distribution in colour-colour diagrams (CC), and thus make reddening/metallicity detects difficult. In some cases such obstacles can be overcome by limiting the errors of the $(U-B)$. Due to these well-known reasons, using U -filter observation is discouraging for most researchers, and they prefer to use $BVRI$

filters. In this sense NGC 1513 is a poorly studied OC in the literature with U -filter observation. The only study with CCD U -filter in the literature is from Sagar et al. (2022) (hereafter S22).

For deriving the reddening of the OCs via the CC diagrams, Q method as the reddening-independent quantity is utilised for young OCs with early type stars (especially B-type stars), whereas for the old-aged OCs with AFGK-type stars, a de-reddened ZAMS (Zero Age Main Sequence) fit is applied to the observations.

In this paper we contribute to the literature for the mentioned deficiency above with the recent CCD $UBV(RI)_{KC}$ photometry of the open cluster, NGC 1513 which resides in Perseus spiral arm (Fig. 1). As stated by Schuster et al. (2007); Tapia et al. (2010); Akkaya Oralhan et al. (2015), since the OCs within the Sierra San Pedro Mártir National Astronomical Observatory (SPMO, hereafter) Open Cluster Survey have been selected to be small or comparable to the size of the field of view of the CCD, the central part of each cluster can be isolated to increase the contrast of the cluster with respect to field stars in the various CC and colour-magnitude diagrams (CMD). In this respect, the SPMO survey has the advantage for identifying various groups of stars in CC and CMD plots, such as red giant/red clump (RG/RC) stars and possible Blue Stragglers. Note that RG/RC stars are also quite important for determining the ages and especially the distances of the clusters.

* E-mail: karatas@istanbul.edu.tr

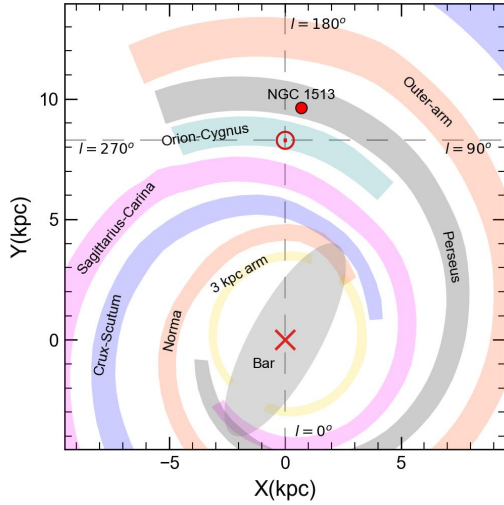


Figure 1. Spatial distribution of NGC 1513 (filled red circle). The schematic projection of the Galaxy with its spiral arms is seen from the North pole. (X, Y) kpc shows the galactocentric cartesian coordinates. The sun is at 8.2 kpc.

On the side of dynamical evolution, the members of the OCs undergo the internal and external perturbations such as stellar evolution, two-body relaxation, mass segregation, tidal interactions with the Galactic disc and bulge, spiral arm shocks, Galactic tidal field, and collisions with GMCs (Lamers & Gieles 2006; Gieles et al. 2007). As stated by Tarricq et al. (2022) (hereafter T22), old OCs are more mass segregated than young OCs. In the sense low-mass stars should be moved to the outer parts of the OCs, whereas massive stars sink into their central parts. This is known as mass segregation. Internal dynamics can shape clusters cores after 100 Myr, while younger OCs inherit their shape from the initial conditions of the cluster formation. The collisions with massive GMCs, tidal effects from spiral arms, disc and Bulge crossings are known as the external perturbations, whereas internal processes are two body relaxation and mass segregation.

The constructed relations among the dynamical indicators c , R_{core} , $RRDP$, R_h/R_t , R_{core}/R_h , R_h/R_t and R_h/R_J , τ , t_{rlx} in terms of age and R_{GC} (kpc) make it allow to interpret internal/external dynamical evolution of the OCs. For this, some valuable studies can be given as the following, Schilbach et al. (2006), Camargo et al. (2009), Bonatto (2010), Güneş et al. (2017) (hereafter G17), Piatti et al. (2017a,b), Piatti et al. (2019), Angelo et al. (2020, 2021, 2023) (hereafter A20, A21, A23), and T22. See Sect.10 for the meanings of these parameters.

In light of the information summarized above, we obtain the colour excess, distance, and age of NGC 1513 from both CCD $UBV(RI)_{KC}$ and Gaia DR3 photometric data. The metal abundance of our sample OC for the isochrone selection is determined from the differential grid technique (hereafter DG) (Netopil & Paunzen 2013; Netopil et al. 2015, 2016). Gaia DR3 astrometric/photometric data have also been utilised for the separation of the cluster members, the obtaining of the structural/dynamical parameters, and kinematics. By combining the findings of the astrophysical/structural/dynamical parameters, the dynamical evolution of NGC 1513 is interpreted. Radial migration is also studied from its birth radius.

This paper is organized as follows. CCD $UBV(RI)_{KC}$ photometric analysis of NGC 1513 is given in Section 2. The cluster membership technique is presented in Section 3. The derivation of reddening, distance modulus/distance, ages from both CCD $UBV(RI)_{KC}$

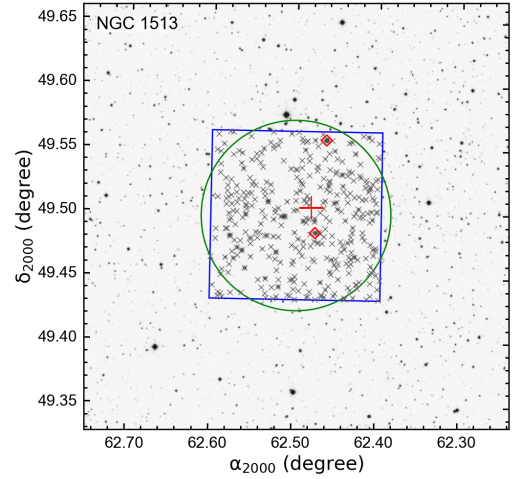


Figure 2. The star chart of NGC 1513 from the webpage of The STScI Digitized Sky Survey. Blue square shows the field of view of the SPM detector, $7.90' (N - S) \times 7.90' (E - W)$ arcmin² which corresponds to $12.350' (N - S) \times 7.887' (E - W)$ arcmin² as the lengths of the field in arcminutes. The cross, big plus and the green circle symbols represent the cluster stars, the central equatorial coordinates (Table 1) and core radius (Col. 5 of Table 7), respectively. Two bright giants are shown by red diamonds (See Sect. 5).

and Gaia DR3 photometries are presented in Sections 4-6. Structure parameters, kinematics, orbital parameters, mass/mass function slope, dynamical parameters, and radial migration are mentioned in Sections 7-10. A Discussion/Conclusion is presented in Section 11 together with a comparison with the literature.

2 OBSERVATION AND DATA REDUCTION

Observation of NGC 1513 cluster and some Landolt standard fields were carried out at the SPMO during the very photometric nights of December 3-5, 2023 UT using the 0.84-m ($f/15$) Ritchey-Chretien telescope equipped with the Mexman filter wheel and a detector (a 2048x2048 13.5- μm square pixels E2V CCD42-40 with a gain of $1.39 \text{ e}^-/\text{ADU}$ and a readout noise 3.49 e^-). Binning 2×2 was employed and the combination of telescope and detector ensured an unvignetted field of view of 7.90×7.90 arcmin². NGC 1513 was observed through the Johnson's UBV and the Kron-Cousins' RI filters with short and long exposure times in order to properly record both bright and faint stars in the region. Its star chart is displayed in Fig. 2. Standard star fields (Landolt 2009) were also observed at zenith ≈ 60 degrees and at meridian to properly determine the atmospheric extinction coefficients. The log of the observations in Table 1 contains the central equatorial/Galactic coordinates, air mass range during the observation, and exposure times in each filter. The flat fields were taken at the beginning and end of each night, and bias images were recorded between cluster observations. Data reduction was carried out by Raul Michel with the IRAF/DAOPHOT¹ package (Stetson 1987). Standard magnitude for a given filter λ is obtained using the following relation.

$$M_\lambda = m_\lambda - [k_{1\lambda} - k_{2\lambda}C]X + \eta_\lambda C + \zeta_\lambda \quad (1)$$

¹ IRAF is distributed by the National Optical Observatories, operated by the Association of Universities for Research in Astronomy, Inc., under cooperative agreement with the National Science Foundation.

Table 1. Equatorial/Galactic coordinates and observation summary of NGC 1513.

α (2000) (h m s)	04 10 00.0
δ (2000) ($^{\circ}$ ' '')	+49 29 27.6
ℓ ($^{\circ}$)	152.59
b ($^{\circ}$)	-01.59
Airmass	1.054 – 1.060
U (Exp.Time (s))	10, 100, 1000
B (Exp.Time (s))	6, 60, 600
V (Exp.Time (s))	4, 40, 400
R (Exp.Time (s))	2, 20, 200
I (Exp.Time (s))	2, 20, 200

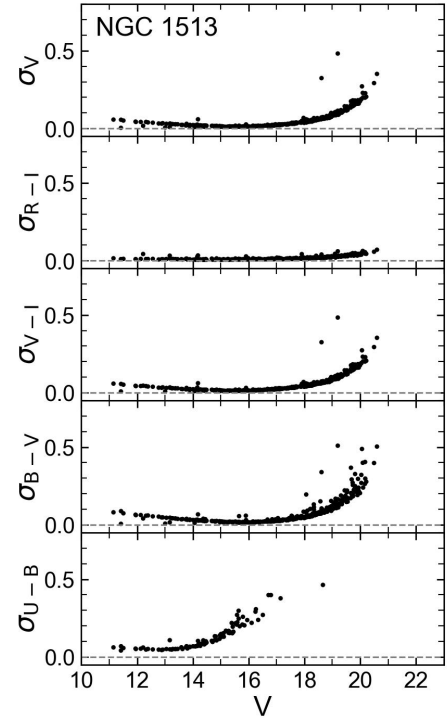
where m_{λ} , $k_{1,\lambda}$, $k_{2,\lambda}$, C , and X are the observed instrumental magnitude, primary/secondary extinction coefficients, colour index and air mass, respectively. M_{λ} , η_{λ} , ζ_{λ} are standard magnitude, transformation coefficient and photometric zero point, respectively. More details on data reduction together the extinction coefficients and zero points for $UBVRI$ filters can be found in the papers of [Akkaya et al. \(2010\)](#), [Akkaya Oralhan et al. \(2015\)](#) and [Akkaya Oralhan et al. \(2019\)](#). The photometric errors in V and colours ($R - I$), ($V - I$), ($B - V$), ($U - B$) against V for NGC 1513 are presented in Fig.3. The mean errors for V -mag intervals are listed in Table 2. Stars towards fainter magnitudes have errors larger than ~ 0.10 mag in both magnitude and the colours. Larger errors of σ_{U-B} as expected are seen at $V > 15$.

The photometry for NGC 1513 is compared to the *CCD UBV* photometry of S22. The cross-identification of the photometric catalogues of our and S22 are correctly matched by taking into consideration the difference with $< 1''$ in $\Delta\alpha$ and $\Delta\delta$. The differences of ΔV and $\Delta(B - V)$ against $(B - V)$ for 64 common stars, and the difference of $\Delta(U - B)$ against $(U - B)$ for 40 common stars are displayed in Fig. 4. The mean differences together dispersions of V and $(B - V)$ are $\Delta V = +0.023 \pm 0.060$ mag and $\Delta(B - V) = +0.021 \pm 0.031$ mag, respectively. For the interval of $0.6 < (B - V) < 1.4$, the majority of the differences of V magnitudes are less than ~ 0.05 mag, except for a few scattered stars. $(B - V)$ values of this paper are in good consistent with S22 at level of $\Delta(B - V) = +0.021$ mag (panel b). In panel (c) there appears a discrepancy between -0.10 mag to -0.50 mag in $(U - B)$ between our and S22 observations. The difference $\Delta(U - B) = -0.16 \pm 0.17$ mag indicates that the $(U - B)$ values of SPMO are bluer than S22. For bright giant (red diamond), the discrepancy is quite small about 0.04 mag in ΔV and -0.01 mag in $\Delta(B - V)$. U -magnitudes of SPMO appear to be brighter than S22. The potential reasons for large colour difference between $(U - B)$ of present photometry and S22 may be due to the used number of the standard fields, the used different effective wavelengths of U -filters, the different reduction techniques, and the so-called red leak in the used U filter. Note that this paper and S22 use U filters of Johnson's and Bessell's.

[Gaia Collaboration Montegriffo et al. \(2023b\)](#) obtained Gaia Synthetic Photometric (GSP) data-base for various photometric filters by utilising the externally calibrated fluxes of the Gaia DR3 *BP* and *RP*. Their GSP data-base allow exquisite photometric calibration of ground-based data-sets. To see the performance of the GSP synthetic *UBVRI* photometry for Johnson-Kron-Cousin system, we plot the magnitude differences of *UBVRI* for the cluster members of NGC 1513 in common with the GSPC (Fig. 5). The differences between U -magnitudes of SPM (filled red dots) and GSP have been plotted against SPMO- V mag. ΔU difference in general fluctuate

Table 2. The mean photometric errors of V , ($R - I$), ($V - I$), ($B - V$) and ($U - B$) for NGC 1513 in terms of V mag.

NGC 1513					
V	σ_V	σ_{R-I}	σ_{V-I}	σ_{B-V}	σ_{U-B}
11 - 12	0.042	0.010	0.044	0.063	0.056
12 - 13	0.034	0.014	0.038	0.053	0.050
13 - 14	0.023	0.010	0.025	0.035	0.059
14 - 15	0.018	0.009	0.020	0.028	0.093
15 - 16	0.013	0.009	0.014	0.020	0.190
16 - 17	0.018	0.010	0.019	0.022	0.303
17 - 18	0.032	0.014	0.034	0.040	0.377
18 - 19	0.062	0.019	0.063	0.082	0.463
19 - 20	0.131	0.033	0.133	0.182	–
20 - 21	0.232	0.052	0.234	0.351	–

**Figure 3.** The distribution of the photometric errors of V , ($R - I$), ($V - I$), ($B - V$) and ($U - B$) against V mag.

around the value -0.09 for $11 < V < 14$, increasing somewhat fainter magnitudes. As for the discrepancies with S22, there appears to be good concordance up to $V = 14.50$ for only three stars but the differences increase towards the fainter magnitudes. For $V > 15$, SPMO- B magnitudes are systematically bluer at a level of ~ 0.03 mag relative to the GSP. The discrepancies for V , R I -magnitudes are satisfactorily small with small wiggles for entire V -mag range. As is evident from their fig.5 of [Gaia Collaboration Montegriffo et al. \(2023b\)](#), the sensitivity of *BP* spectrophotometer for $\lambda < 400$ nm is low and multi-structured with two steep branches at ~ 330 nm and ~ 390 nm. In the sense, the U magnitudes from both ground-based and space-based fluxes in ultraviolet (UV) region are always problematic, and thus *BP* performance of Gaia DR3 in the UV filter is not satisfactory good. Whereas *RP* appears to give more consistence synthetic magnitudes with the observations.

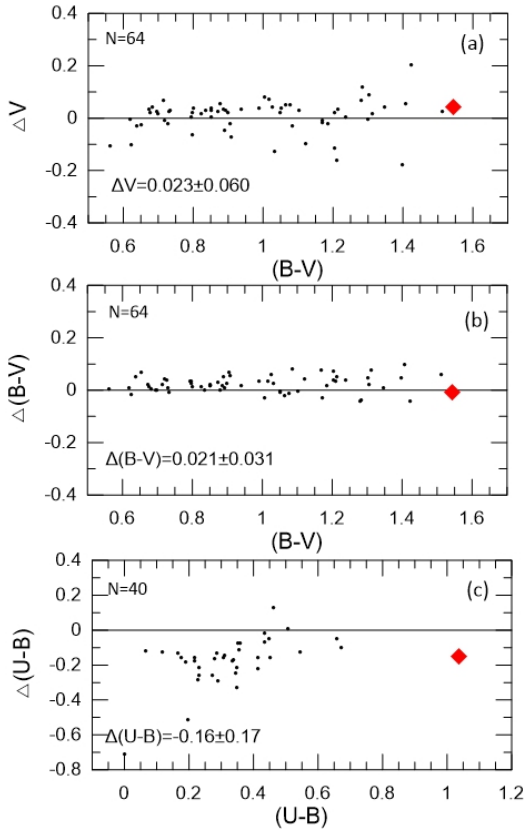


Figure 4. The differences of V -mag, $(B - V)$ and $(U - B)$ as a function of $(B - V)$ and $(U - B)$. Δ means this paper – S22. Red diamond denotes the bright giant (*LAMOST* – 695710060) for just presentation (for the symbol, see also Figs. 6 and 8).

3 MEMBERSHIP SELECTION

In order to separate the cluster members of NGC 1513, its Gaia DR3 astrometric/photometric data (Gaia Collaboration Vallenari et al. 2023a) for a large-area (15 arcmin) from VizieR² are utilised. On the (μ_α, μ_δ) , the potential cluster members present a more concentrated structure, whereas field stars have a more scattered distribution. We applied the Gaussian Mixture Model (GMM) and SCIKIT-learn package (Pedregosa et al. 2011) to the cluster stars, and thus their membership probabilities $P(\%)$ have been determined. The GMM³ model considers that the distribution of proper motions of the stars in a cluster’s region can be represented by two elliptical bivariate Gaussians. The expressions used can be found in the papers of Balaguer-Nunez et al. (1998), Wu et al. (2002), Sariya et al. (2012), Dias et al. (2018), Cakmak et al. (2021), and Cakmak & Karatas (2022). The first significant rise ($> 50\%$) in the membership probability histogram is taken into account as the membership percentage. The estimated median equatorial coordinates from the likely members are listed in Table 1. We find its median Gaia-DR3 parallax $\varpi = 0.679 \pm 0.048$ mas. This parallax value is corrected for the Gaia DR3 parallax zero-point, -0.021 mas offset given by Groenewegen (2021). The distance of NGC 1513 is obtained as 1435 ± 14

² <http://vizier.u-strasbg.fr/viz-bin/VizieR?-source=II/246>.

³ P is defined Φ_c / Φ . Here $\Phi = \Phi_c + \Phi_f$ is the total probability distribution. c and f subscripts for cluster and field parameters, respectively. The used parameters for estimation of Φ_c and Φ_f are $\mu_\alpha, \mu_\delta, \varpi, \sigma_{\mu_\alpha}, \sigma_{\mu_\delta}, \sigma_\varpi$.

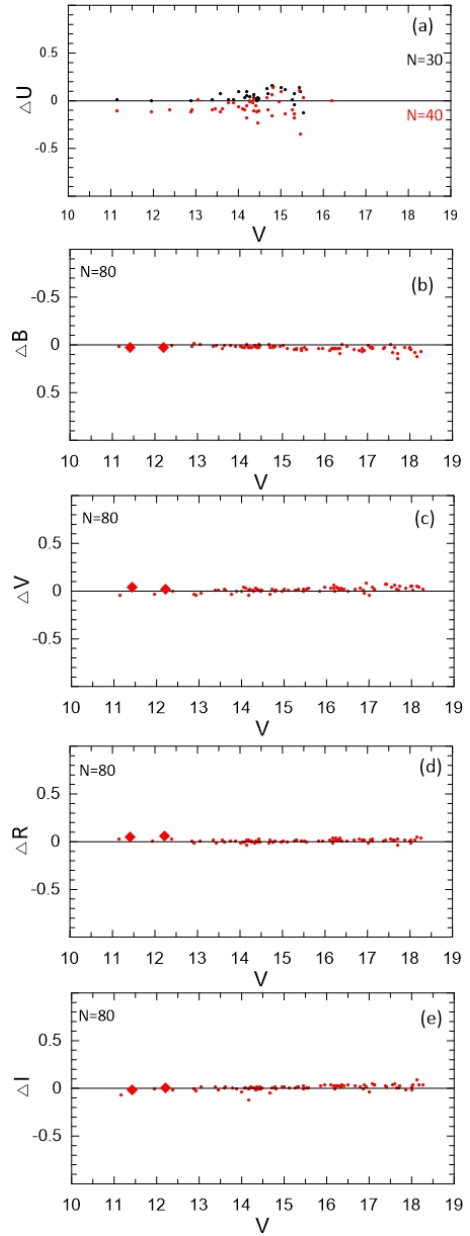


Figure 5. The differences of the magnitudes of $UBVRI$ against SPM- V -mag. Δ means between SPMO and GSP. In panel (a), comparison with S22 is also shown with the filled black dots. Red diamonds denote two bright giants.

pc from the posterior probability density functions (PDFs)⁴ given by Bailer-Jones et al. (2018). The inverse parallax relation gives a distance, 1520 ± 111 pc. However the discrepancy of both distances is quite small, 85 pc. The median proper motion components, the median parallax/bayesian distance, and the number of the members of NGC 1513 are listed in first row of Table 3. Within the errors its median values are in compatible with the one of Cantat-Gaudin et al. (2020) (bottom panel).

Once we assigned the cluster membership probabilities, we cross-matched the coordinates (α, δ) of cluster stars in our ground-base photometric data with those in Gaia DR3. We set 1 arcsec as the maximum difference in (α, δ) for merging both data-sets.

⁴ <https://www2.mpa-hd.mpg.de/calj/gedr3-distances/main.html>

Table 3. The median proper motion components and parallax/distance, and the number of the probable members derived by us (top row) and Cantat-Gaudin et al.(2020) (bottom row).

Cluster	μ_α (mas/yr)	μ_δ (mas/yr)	ϖ (mas)	d (pc)	N
NGC 1513	1.31 ± 0.11	-3.70 ± 0.10	0.679 ± 0.040	1435 ± 14	482
	1.32 ± 0.18	-3.68 ± 0.16	0.650 ± 0.060	1540 ± 310	332

4 DERIVATION OF REDDENING

The reddening of NGC 1513 is determined from 35 early type members (relatively large red dots) with $V < 15$ mag and $\sigma_{U-B} \leq 0.10^5$ on the CC (Fig. 6). $E(B-V)$ values of the members have been estimated by using the intrinsic colour relation of early type stars in tables 2-3 of Sung et al. (2013) (hereafter S13). The following equations of $(B-V)_o = 0.328Q - 0.019$, $Q = (U-B) - 0.72(B-V) - 0.025E(B-V)^2$, and $E(U-B) = 0.72E(B-V) + 0.025E(B-V)^2$ of S13 have been applied to the members. The median reddening is obtained as $E(B-V) = 0.79 \pm 0.09$ mag. Thus the reddened colour sequence of S13 (red curve) is fitted to the members (Fig. 6). The selected 35 members almost present a tight distribution around the reddened S13 main-sequence.

To test the reddening law of NGC 1513, we estimated the colour excess ratios $E(V-\lambda)/E(B-V)$ of the members from the intrinsic colour relation of S13. Thus, the total-to-selective extinction ratio R_V is obtained from the relation between R_V and colour excess ratios $E(V-\lambda)/E(B-V)$ of optical-near infrared colours, given by Guetter & Vrba (1989). The obtained colour excess ratios are listed in Table 4. The weighted average R_V is estimated as 2.85 ± 0.05 (Table 4). This value implies that the reddening law toward NGC 1513 ($\ell = 152^\circ.59$, $b = -1^\circ.59$) is slightly low as compared to standard $R_V = 3.1$ and also the mean value $R_V = 3.18$, given by (Buser 1978) for spectral type, $B3V-B8V$. However, the interstellar reddening law R_V is known to be different for different sightlines (Fitzpatrick & Massa 2009). As discussed by S13, many young OCs are known to show an abnormal reddening law. Sung & Bessell (2014) also confirmed the variation of R_V with Galactic longitude from optical and 2MASS data of 162 young OCs (see their fig. 2). They report that the young OCs in the Perseus arm have relatively small R_V values (~ 2.9). Note that NGC 1513 resides in Perseus spiral arm (see Fig. 1).

To de-redden the two late-type bright giants, their intrinsic $(B-V)_o$ colours are obtained by utilising the spectral type- T_{eff} relation in table 5 of S13. Their estimated reddening values are $E(B-V) = 0.66 \pm 0.05$ mag and $E(B-V) = 0.70 \pm 0.05$ mag, respectively (row 7 of Table 5). Thus, the giant intrinsic sequence of S13 for the two giants is reddened by amount of $E(B-V) = 0.68$ mag (Fig. 6). We also determined their reddenings from table II of Fernie (1963) as $E(B-V) = 0.69 \pm 0.09$ mag and $E(B-V) = 0.70 \pm 0.05$ mag. Both the two detects are in pretty compatible.

The spatial variation of reddening of NGC 1513 which is derived from its member stars is presented in Fig. 7. The coloured contours as iso-reddening represent different amounts of reddening $E(B-V)$. Judging by the map in Fig. 7 and the mean $E(B-V) = 0.79$ mag, there may be variations of ~ 0.10 mag across the field of NGC 1513. Although non-negligible this variation does not affect significantly

⁵ σ_{U-B} and σ_{B-V} errors of the cluster stars are generally selected to be less than 0^m10 , frequently $\leq 0^m05$, on the $(U-B)$, $(B-V)$ diagram (CC) to allow us reasonable $E(B-V)$ and photometric $[M/H]$ detects. The errors of σ_{U-B} are also always larger than the ones of σ_{B-V} , due to the smaller sensitivity of the CCD in the ultraviolet.

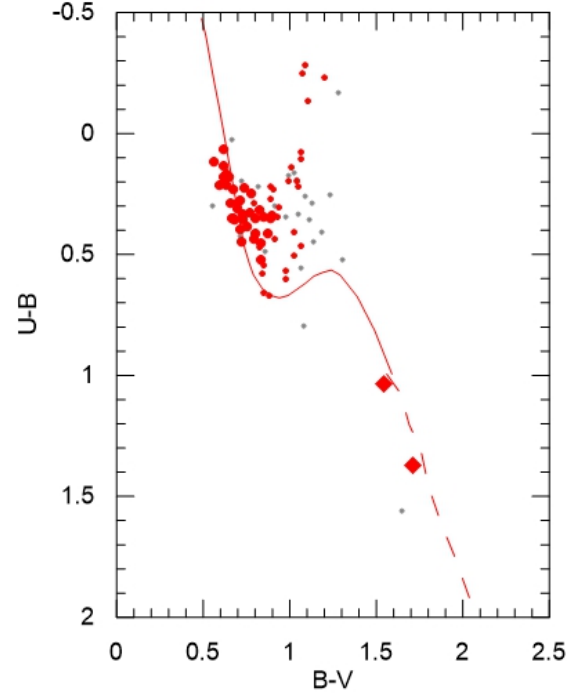


Figure 6. The CC diagram for 35 early -type members (large red dots) with $\sigma_{U-B} \leq 0.10$. The relatively small red and gray dots show 16 members with $\sigma_{U-B} > 0.10$ and 95 member/non-members, respectively. Red solid/dashed curves, and red diamonds represent the reddened S13 dwarf/giant sequences, and bright evolved giants, respectively.

Table 4. $E(V-\lambda)/E(B-V)$ ratios (Col. 2) in terms of four colour indices (Col. 1). R_V is the weighted average of four colours. Here λ is I, J, H and K_s . N (last column): early type member numbers.

Colour	$E(V-\lambda)/E(B-V)$	N
V-I	1.198 ± 0.038	35
V-J	2.076 ± 0.090	35
V-H	2.404 ± 0.10	35
V- K_s	2.574 ± 0.15	35
$R_V = 2.848 \pm 0.054$		

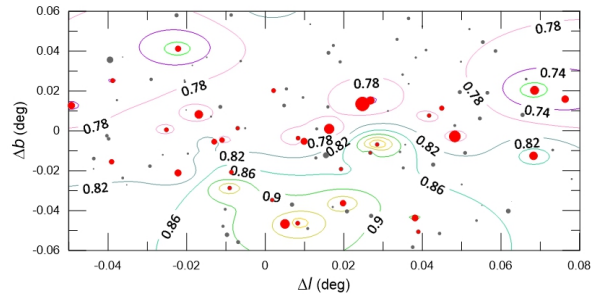


Figure 7. Reddening map of NGC 1513. Red and gray dots shows the member and non-member cluster stars, respectively. The size of the dots is scaled to the V -mag of the star. The coloured line types as iso-reddening contours represent different amounts of reddening $E(B-V)$.

Table 5. Information of the two bright giants in NGC 1513. The photometry of Frolov et al (2002) and Sagar et al (2022) is also presented for the comparison.

	LAMOST 695710060	2MASS J04095395+4929043	
	NGC-1513 RH88	NGC-1513 RH 62	Reference
V	11.420	12.216	This study
	11.400	12.230	F02
	–	12.173	S22
(B – V)	1.709	1.545	This study
	1.640	1.430	F02
	–	1.552	S22
(U – B)	1.372	1.035	This study
	–	1.188	S22
α (2000) (h m s)	04 09 51.041	04 09 53.970	
δ (2000) ($^{\circ}$ ' '')	+ 49 33 25.270	+49 29 04.45	
Membership	0.99	0.99	
$E(B - V)$	0.70	0.66	
$m (M_{\odot})$	3.66	3.45	
M_V	-1.45	-0.66	
ϖ (mas)	0.702±0.015	0.796±0.021	
$(\mu_{\alpha}, \mu_{\delta})$ (mas/yr)	(+1.201, -3.736)	(+1.259, -3.648)	
V_{rad} (km/s)	-15.198±0.178	-15.18±0.39	
[Fe/H]	-0.088	–	
d_{plx} (pc)	1425±30	1256±33	
d_{ph} (pc)	1496±105	1581±101	

the result. Most young OCs with ages younger than 10 Myr show a differential reddening across the field of view. But for relatively old OCs, it is not well known whether there is a differential reddening across the cluster or not. That is the reason to check the differential reddening across the cluster.

5 METAL ABUNDANCE AND BRIGHT GIANTS OF NGC 1513

The metal abundance of NGC 1513 has been obtained by using the DG technique developed by Pöhl and Paunzen (2010), and improved by Netopil & Paunzen (2013); Netopil et al. (2022). The details of the DG method can also be found in the papers of Netopil et al. (2016); Netopil et al. (2022). For this, the photometric data of main-sequence stars of NGC 1513 have been transformed to luminosities and mean effective temperatures, the latter based on up to five colour indices using 2MASS (Skrutskie et al. 2006), Gaia DR3, and our photometric data. These have been compared to ZAMS normalised B12 PARSEC isochrones. The DG method derives its metal abundance as $[Fe/H] = -0.06 \pm 0.15$ ($Z = +0.013 \pm 0.004$).

The identification names of the two bright giants in Fig. 6 has been taken from SIMBAD database as 2MASS J04095395+4929043 (NGC 1513 RH62) and LAMOST 695710060 (Gaia DR3 247308962849970560) (NGC 1513 RH88). The information of photometry, membership probability, reddening, mass/absolute magnitude, Gaia astrometry/Gaia radial velocities, metal abundance, Gaia/photometric distances are listed in Table 5. LAMOST database give the astrophysical parameters of the bright giant LAMOST 695710060 as $T_{eff} = 4493$ K, $\log g = 2.2$, and $[Fe/H] = -0.088$. This value is in good agreement with -0.06 dex (the DG method). Its T_{eff} and $[Fe/H]$ are also in compatible with the $T_{eff} = 4786$ K and $\log g = 2.07$ which the MIST/MESA isochrone gives.

The two giant members with high membership probabilities (row 6 of Table 5) remain within SPMO FOV (see Fig. 2). Frolov et al. (2002) (hereafter F02) identify these two bright giants in late-

evolution stages in their CMD (see their fig.5), whereas S22 identify only one bright giant-2MASS J04095395+4929043 (NGC 1513-RH62) (see their fig.7). The positions of the bright giants in Fig. 11(a) coincide with the photometric data of three studies.

F02 give their absolute magnitudes as $M_V = -0.41$ and $M_V = -1.20$ with the aid of the isochrone of Girardi et al. (2000). These values are not too different from our detects (row 9 of Table 5). It appears that 2MASS J04095395+4929043 (NGC 1513 RH62) is a red giant in the helium-burning stage of stellar evolution, and the other giant- LAMOST-695710060 (NGC 1513 RH88) may be a asymptotic giant (AGB) with helium and hydrogen shell burning, depending on its position on the CMD. Their Gaia astrometric values are agreement with the median values in Table 3 within the error limits.

6 AGE AND DISTANCE OF NGC 1513

We used MIST isochrones (MESA Isochrones and Stellar Tracks) to derive distance modulus and age of NGC 1513. These isochrones are based on the Modules for Experiments in Stellar Astrophysics (MESA) code (version v7503)¹ (Choi et al. 2016; Dotter et al. 2016) and (Paxton et al. 2011, 2013, 2015, 2018). The metal abundance ($[Fe/H]$, Z) = $(-0.06, +0.013)$ of the DG method is considered for selecting the isochrones. Due to the diversity of the rotational velocity even in a cluster (Lim et al. 2019), the main-sequence turn-off broadens. The broadening in the main sequence of the CMD is also responsible for binarity, peculiarity, rotation in the stars. By taking into consideration this fact, the MIST/MESA isochrones with $Z = +0.013$ for both $V/V_{crit} = 0.4$ (rotation) and $V/V_{crit} = 0$ (no-rotation) have been fitted to the five CMDs: V , $(B - V)$, V , $(U - B)$, V , $(R - I)$, V , $(V - I)$, and G , $(G_{BP} - G_{RP})$ (Fig. 8a-e). The reddenings $E(R - I)$, $E(V - I)$, and $E(G_{BP} - G_{RP})$ have been obtained from the corresponding $E(B - V)$ value via the following relations of $E(V - I) = 1.198E(B - V)$ (Table 5), $E(R - I) = 0.69E(B - V)$ (Straizys 1995), and $E(B - V) = 0.775E(G_{BP} - G_{RP})$ (Bragaglia et al. 2018). Note that the coefficient 1.198 is quite close to 1.25 given by Dean et al. (1978). The estimated reddenings for the colours (Col. 1) are listed in Col. 2 of Table 6. A visual extinction of $A_V = 2.85 \times E(B - V)$ is applied to the absolute magnitudes of the isochrones. The MIST/MESA isochrones have been shifted both vertically and horizontally to the amounts of five colour-excesses on the CMDs (Fig. 8) until the best fit to the observed intermediate section of the main sequence (MS) as well as the RG/RC sequences is obtained. This vertical shift is the true distance modulus, $DM_o = (V_0 - M_V)$. The derived distance moduli ($V_0 - M_V$) and distances d (pc) for five colours are given in Cols. 3-4 of Table 6. For the determination of the age, the MIST/MESA isochrones have been shifted both vertically and horizontally in the CMD's with $M_V + 2.85E(B - V) + DM$ and $C_0(\lambda_1 - \lambda_2) + E[C(\lambda_1 - \lambda_2)]$, respectively. The derived ages are given in Col. 5 of Table 6. The MIST/MESA isochrones with rotation/no-rotation closely match the observational data in the CMDs (Fig. 8), and provided consistent ages and distances (Table 6). We report an age of 224 ± 27 Myr from $V - (B - V)$ for NGC 1513.

The main sequence strips or bands in the CMDs are affected by the contamination of binary stars, particularly the mid-points due to stellar binaries. For this reason, we have fitted MIST/MESA isochrones to the blue- and faint-most side of the observed sequences whenever

¹ <https://waps.cfa.harvard.edu/MIST/interp-isos.html>

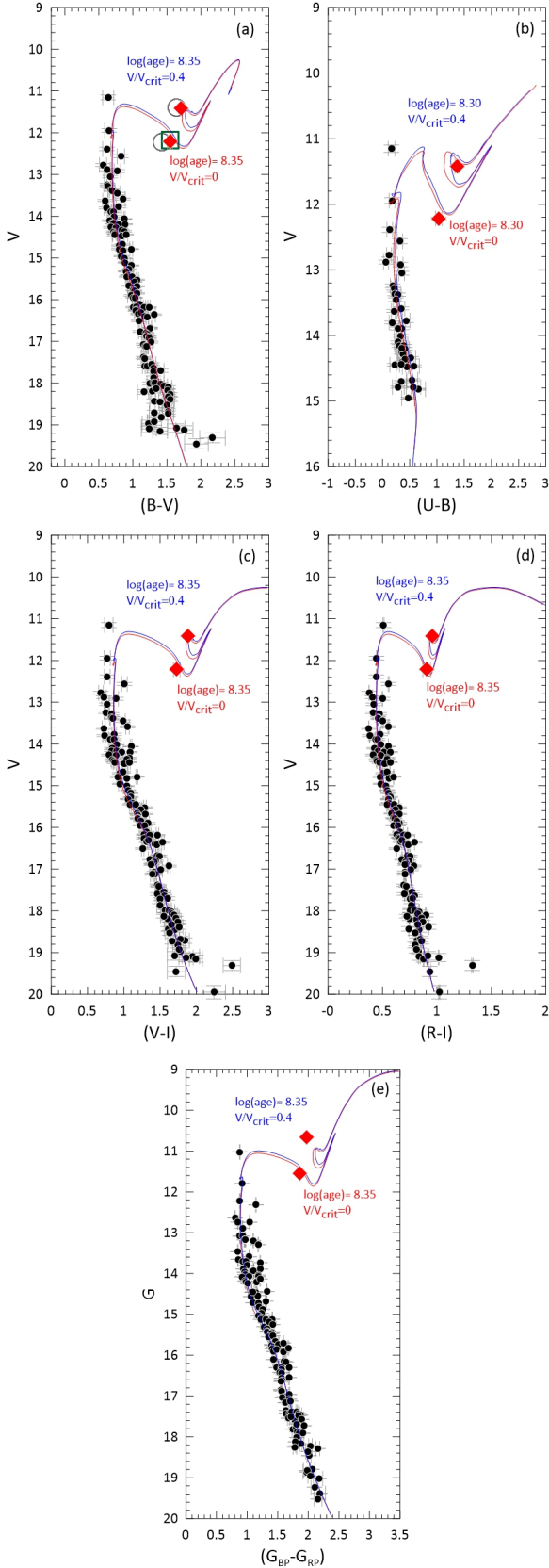


Figure 8. The V-(B-V) (127 members), V-(U-B) (43 members), V-(V-I) (127 members) and V-(R-I) (127 members) and G- (G , $G_{BP} - G_{RP}$) (147 members) CMDs of NGC 1513. Red diamonds show the bright giants of this study. Large circles and a large square in upper left panel represent the ones of F02 and S22 (See Table 5), respectively.

Table 6. Derived astrophysical parameters of NGC 1513. CE means the colour excess.

NGC 1513	CE	$(V - M_V)_o$	d(pc)	Age (Myr)
(B-V)	0.79 ± 0.08	10.90 ± 0.15	1514 ± 105	224 ± 27
(U-B)	0.58 ± 0.06	10.90 ± 0.20	1514 ± 140	200 ± 82
(V-I)	0.96 ± 0.11	10.90 ± 0.15	1514 ± 105	224 ± 58
(R-I)	0.55 ± 0.06	10.90 ± 0.20	1514 ± 140	224 ± 58
$(G_{BP} - G_{RP})$	0.95 ± 0.11	10.90 ± 0.15	1514 ± 105	224 ± 58

possible, assuming that it reflects the single-star distribution (Carney 2001).

As we experienced in Akkaya et al. (2010), the uncertainties of distance moduli and ages of our sample OC have been derived with the help of two MIST/MESA isochrones on the CMDs.

For the comparisons with the literature, we have considered mostly the astrophysical parameters given by $(B - V)$ colour index, because the astrophysical parameters of the OCs are mostly given, and best represented, in terms of the CMD: $V - (B - V)$. For this, a summary of the astrophysical parameters and the comparison to the literature for our sample OC are listed in Table 10.

The distance modulus/distance of NGC 1513 are also obtained by utilising the reddening-independent quantities, Q' , Q_{VJ} , Q_{VJ} , Q_{VH} and Q_{VK_S} from 35 early type stars. These quantities are nearly free from metallicity differences. The ZAMS of S13 in the $Q_{V\lambda} - Q'$ plots should be fitted to the lower ridge of the main-sequence band to avoid the effects of multiplicity and evolution, as stated by Lim et al. (2014). The ZAMS line is shifted up and down in the $Q_{V\lambda} - Q'$ plots by 0.1 mag. The error of this method is about 0.20 mag. Once the adjustment of ZAMS above and below the distribution of the members, its distance modulus from four colour indices is obtained as $(V_0 - M_V) = 10.90 \pm 0.20$ mag, equivalent to 1514 ± 140 pc. Within the error limits this distance falls in the distance range of Gaia DR3 parallax (Table 4) and $V - (B - V)$ (Table 6).

7 STRUCTURAL PARAMETERS

The stellar radial density profile (RDP) of NGC 1513 is constructed from the Gaia DR3 photometric/astrometric data for cluster field within $15'.0$ down to $G = 19$ mag (Arenou et al. 2018). The R_{core} , σ_{bg} , and σ_0 of NGC 1513 have been derived by fitting two-parameter model of King (1966) to the observational RDP (Fig. 9). The two-parameter function (King 1966) is given as below.

$$\sigma(R) = \sigma_{bg} + \frac{\sigma_0}{1 + \left(\frac{R}{R_{core}}\right)^2}$$

For this equation, σ_{bg} is the residual background density. σ_0 and R_{core} are the central density of stars and the core radius, respectively. The cluster radius (R_{RDP}) by comparing the RDP level with background and by measuring the distance from the centre is determined (Bonatto & Bica 2007). The R_{RDP} is taken as an observational truncation radius, whose value depends both on the radial distribution of member stars and the field density. The large uncertainty within $R < 1'$ in the RDP of NGC 1513 is owing to its low star content in its central part. The three-parameter model of King (1962) describes well the outer parts of a cluster, while the two-parameter model of King (1966) explains the central region of the clusters, as discussed by Bonatto et al. (2005). Its tidal radius R_t has been obtained as 10.65 pc by applying the three-parameter King function to the observational RDP (Fig. 9). These structural parameters and their

Table 7. Structural parameters of NGC 1513.

Cluster	(l')	σ_{0K}	σ_{bg}	R_{core}	R_{RDP}	σ_{0K}	σ_{bg}	R_{core}	R_{RDP}	R_t	CC
	(pc)	(* l'^{-2})	(* l'^{-2})	(l')	(l')	(* pc^{-2})	(* pc^{-2})	(pc)	(pc)	(pc)	
(1)	(2)	(3)	(4)	(5)	(6)	(7)	(8)	(9)	(10)	(11)	(12)
NGC 1513	0.439	7.02 ± 2.58	4.63 ± 0.16	4.46 ± 0.93	11.26 ± 0.42	3.08 ± 1.13	2.02 ± 0.07	1.96 ± 0.41	4.94 ± 0.19	10.65	0.956
								1.41 ± 0.74	3.50 ± 1.80		1
								1.43 ± 0.21	6.68 ± 0.67		2
								1.65 ± 0.26	6.51 ± 0.20		3
								2.00 ± 0.37		5.48 ± 0.70	4
								1.94		10.63	5

Notes: (* l'^{-2}) and (* pc^{-2}) in Cols. 3-4 and 7-8 represent *stars arcmin⁻²* and *stars pc⁻²*, respectively. For the radius in pc we adopt the Gaia distance (Table 6). R_t in Col. 11 represents the tidal radius and Col. 12 means the correlation coefficient of the RDP fit. The first row lists our results, the subsequent ones literature data - References: 1: Maciejewski and Niedzielski (2007), 2: Bukowiecki et al. (2011), 3: Güneş et al. (2017), 4: Kharchenko et al. (2013), 5: Hunt & Reffert (2024).

meanings together with the literature values are listed in rows 2-11 of Table 7.

Our R_t is in good agreement with the value of Hunt & Reffert (2024), which is based on Gaia DR3 data. The value of Kharchenko et al. (2013) are smaller than our value. As emphasized by T22, the obtaining of the tidal radii of the OCs is quite difficult, owing to both the loose nature of the OCs and the contamination by field stars. Our (R_{core} , R_{RDP}) (pc) falls within or are close to the values of Maciejewski and Niedzielski (2007), Bukowiecki et al. (2011), G17, Kharchenko et al. (2013), and Hunt & Reffert (2024) within the uncertainties.

The density contrast parameter (δ_c) to estimate the compactness of the OCs is obtained from the relation,

$$\delta_c = 1 + \frac{\sigma_0}{\sigma_{bg}}$$

The δ_c of NGC 1513 is estimated as 2.52 from the information of Cols. 3-4 of Table 7. This value lies outside the range $7 \leq \delta_c \leq 23$ for the compact OCs given by Bonatto (2009). This means that NGC 1513 ($b = -1^\circ.59$) has a sparse OC. Note that different Galactic latitudes have different properties and also suffer from differences in density contrast, since low-Galactic latitude OCs tend to be projected against denser fore/backgrounds. In this context, Bica & Bonatto (2005) also state that the δ_c values of the OCs depend on the Galactic latitude than the cluster mass. Accordingly, the populous and high Galactic latitude OCs have large density contrast parameters.

8 KINEMATICS AND ORBITAL PARAMETERS

The Gaia radial velocities (Table 5) of two bright giants of NGC 1513 have been taken from Soubiran et al. (2018, 2019). The average radial velocity of the two bright giants has been assumed as NGC 1513's radial velocity. Its heliocentric velocity (U, V, W) in the right-hand system has been obtained from its average radial velocity, the median proper motion components/distance of NGC 1513 by using the algorithm of Johnson & Soderblom (1987). Here the photometric distance of Gaia DR3-CMD (Table 6) is adopted. Its space velocity is converted to the components U', V', W' by correcting for the Solar motion (U, V, W) $_{\odot} = (+11.10, +12.24, +7.25)$ km s⁻¹ with respect to the local standard of rest (LSR) (Schönrich and Binney 2010). Here, $R_{\odot} = 8.2 \pm 0.1$ kpc (Bland-Hawthorn et al. 2016) and $V_{LSR} = 239$ km s⁻¹ (Brunthaler et al. 2011) are adopted. The heliocentric cartesian distances (x', y', z') (kpc) and LRS-velocity components (U', V', W') km s⁻¹ are converted to the Galactic Rest of Frame

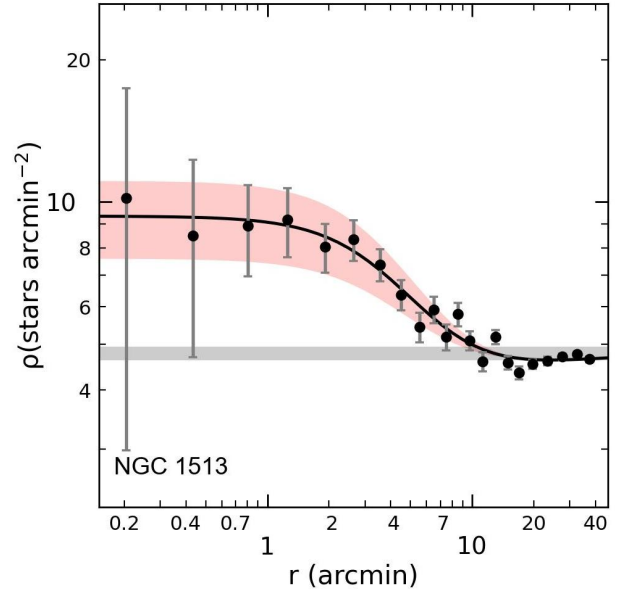


Figure 9. The radial density profile of NGC 1513. Solid line and horizontal gray bar represent the best fit King profile and the stellar background level measured in the comparison field, respectively. The 1σ King fit uncertainty is shown by the shaded domain.

(GSR) i.e., (x, y, z) (kpc) and (V_x, V_y, V_z) km s⁻¹. The azimuthal velocity (V_{Φ}) (km s⁻¹) is estimated via

$$V_{\Phi} = \frac{xV_y - yV_x}{R}$$

Here, $V_{\Phi} < 0$ means prograde. From the "MWPotential2014" code in the galpy-code library¹ written by Bovy (2015), peri and apogalactic distances (R_{min}, R_{max}) (kpc) and the maximum height distance (z_{max}) (kpc) are obtained. The orbital eccentricity (ecc) is estimated via the relation

$$ecc = \frac{R_{max} - R_{min}}{R_{max} + R_{min}}$$

The current mean galactocentric radius R_m is estimated from $(R_{min} + R_{max})/2$, which is also known as the guiding or mean orbital radius. The orbits have been integrated using kinematical parameters (Table 8) for its age (Table 6) within the galactic potential.

¹ <http://github.com/jobovy/galpy>

Table 8. The average radial velocity (V_R) km s^{-1} , space velocity components and rotational velocity (U, V, W, V_Φ) km s^{-1} , eccentricity (ecc) and peri and apogalactic distances, initial and present day distances ($R_{max}, R_{min}, R_m, z_{max}, R_{in}, R_{GC}$) (kpc). The orbital angular momentum (J_z) (kpc km s^{-1}). T is the time of one revolution around the Galactic center as Myr. N_{Rev} is the number of the revolution over the age of the cluster (last row).

NGC 1513	
V_R	-15.38 ± 0.41
U	2.57
V	-29.22
W	-12.59
V_Φ	-222.42
ecc	0.06
R_{min}	8.47
R_{max}	9.57
R_m	9.04
z_{max}	0.08
R_{in}	8.50
R_{GC}	9.57
J_z	-2127.53
T	250
N_{Rev}	1

The galactic potential as the sum of the galactic components is explained by Bovy (2015). Its orbital angular momentum component J_z (kpc km s^{-1}) is calculated from the equation $J_z = xV_y - yV_x$. All these parameters are listed in Table 8.

According to rotational velocity $V_\Phi = 222 \text{ km s}^{-1}$, the eccentricity, 0.06, and orbital angular momentum value (Table 8), NGC 1513 reflects the characteristics of the Galactic disk. The x-y (kpc) plane is known as projected on to the Galactic plane, whereas z-R (kpc) is the meridional plane. On the x-y (kpc) plane (Fig. 10), it follows a circular path around the Galactic center. According to its revolution period ($T=250$ Myr) around the Galactic center (Table 8), it has almost made one revolution around the center of the Galaxy. The gray circles in the panels show its five future revolutions.

The orbits in the z-R (kpc) plane show boxy-like type properties. NGC 1513 moves in the meridional planes within the confined spaces and is oscillating along the z-axis. NGC 1513's orbit is confined in the range of $\sim 8.5 < R_{gc} \leq 9.6$ kpc. Its initial ($t = 0 \text{ Gyr}$) and present day position in our Galaxy are shown in Fig. 10 with the filled blue and red dots, respectively. These positions are calculated by using the "MWPotential2014" in the galpy-code package. For this, time is taken as zero (initial) and cluster age (present day). Its closest approaches to the Sun is at $(d - \text{kpc}, t - \text{Gyr}) = (0.46, 0.014)$.

9 MASS AND MASS FUNCTION SLOPE

The masses of the main sequence members of Gaia DR3 for NGC 1513 have been determined from the MIST/MESA isochrones. G magnitudes of main sequence members have been converted into the absolute magnitudes from its reddening and distance modulus (Cols. 2 and 3 of Table 6). Mass function (MF) is defined as the distribution of masses of cluster stars per unit volume. The mass function in terms of 0.05 bin sizes is given in Fig. 11. The MF slope is fitted to a power-law given by,

$$\log \frac{dN}{dM} = -(1 + \chi) \log(M) + \text{constant} \quad (2)$$

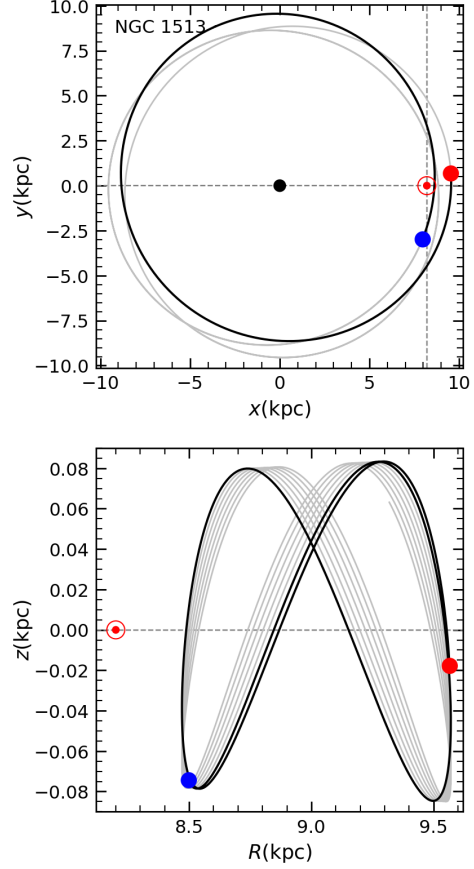


Figure 10. Galactic orbit of NGC 1513. The trajectories represent the paths traveled by the OC through its age. The filled blue/red dots show its initial/present day position. The open red circle shows the Sun's position.

Here dN is the number of cluster members for the mass interval dM with central mass M , and χ is mass function slope. Since Gaia data (G mag) is complete below $G = 19$ mag (Arenou et al. 2018), stars brighter than this limit are taken, which correspond to stars more massive than $1 M_\odot$. Applying Eq. (2) to the observations (Fig. 11) gives NGC 1513's MF slope as $\chi = 2.39 \pm 0.25$. This MF slope is very steep as compared to $\chi = 1.3 \pm 0.7$ of Kroupa (2001) with the uncertainties. Total mass is obtained from the MF slope of NGC 1513. The mass range, MF slope, total mass, mean mass, and member number are listed in Col. 1 of Table 9. Our MFs is steep as compared to $\chi = 1.55 \pm 0.20$ of Maciejewski and Niedzielski (2007), $\chi = +1.90 \pm 0.12$ of G17 and $\chi = 1.53 \pm 0.37$ of S22. The relatively small mass values, $\sim 625 M_\odot$ of this study and $713 M_\odot$ of G17 are almost compatible.

By following the procedure given by Allison et al. (2009) and T22, we estimated the mass segregation ratio Λ_{MSR} from Eq.(3) by using the masses of the members of Gaia DR3 of NGC 1513.

$$\Lambda_{MSR}(N) = \frac{\langle l_{random} \rangle}{l_{massive}} \pm \frac{\sigma_{random}}{l_{massive}}, \quad (3)$$

The degree of mass segregation Λ_{MSR} is the ratio of the lengths of the average randomly selected star (MST) to the most massive star, as explained by Allison et al. (2009). MST is defined as the length of the minimum spanning tree of the most massive stars of a cluster (Allison et al. 2009). $\langle l_{random} \rangle$ is the average length of the MST of N randomly chosen stars, and thus $\langle l_{massive} \rangle$ is the length of the

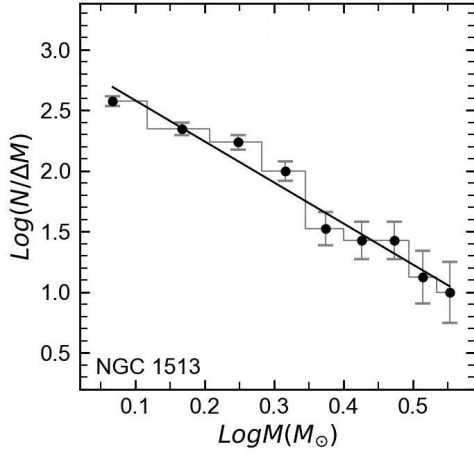


Figure 11. The mass function of NGC 1513. The vertical error bars as poisson noise are proportional to the \sqrt{N} .

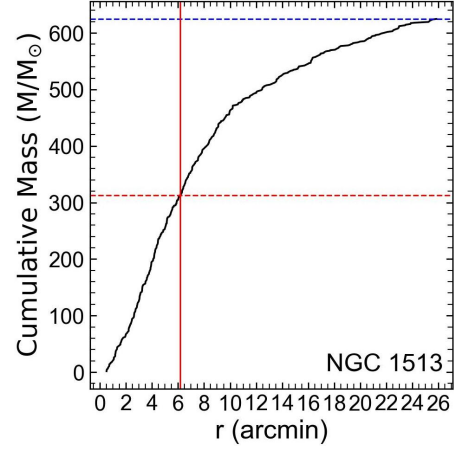


Figure 13. The cumulative mass versus radius of NGC 1513. The vertical line represents the half-mass radius corresponds to the half-mass (horizontal dotted line). The upper blue dotted line denotes the total mass.

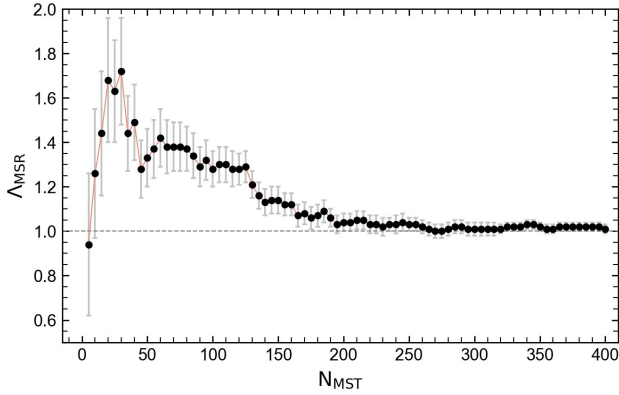


Figure 12. Mass segregation ratio $\Lambda_{MSR}(N)$ for NGC 1513 as a function of the N more massive stars. The horizontal red dotted line denotes the limit $\Lambda_{MSR} = 1$ which means no-mass segregation.

MST of the N most massive stars. σ_{random} is the standard deviation of $\langle l_{random} \rangle$. The length of the MST of the most massive stars ($l_{massive}$) is shorter than the average length of the MSTs of the random stars ($\langle l_{random} \rangle$) (Allison et al. 2009). In this context, the massive stars have more concentrated distribution, hence the cluster is mass-segregated. Allison et al. (2009) state that $\Lambda_{MSR} = 1$, $\Lambda_{MSR} > 1$ and $\Lambda_{MSR} < 1$ indicate no-mass segregation, mass segregation and inverse-mass segregation, respectively.

The relation of Λ_{MSR} versus N_{MST} is displayed in Fig. 12 for NGC 1513. For $N_{MST} < 10$, 10 most massive stars with $\Lambda_{MSR} < 1$ show inverse mass segregation. This method places 50 most massive stars in the inner parts the cluster. Almost 190 most massive stars with $\Lambda_{MSR} > 1$ are mass segregated. This does necessarily mean that these massive stars are widely spaced than the other stars in the cluster. Almost 190 most massive stars with $\Lambda_{MSR} > 1$ are mass segregated. First 40 most massive stars are $\Lambda_{MSR} \sim 1.7$ times closer to each other in the inner radius. For $50 < N < 120$, Λ_{MSR} decreases to ~ 1.35 . Λ_{MSR} drops to unity for around $N_{MST} = 190$. Beyond this limit, no any sign of mass segregation is seen.

10 DYNAMICAL PARAMETERS

The relaxation time t_{rlx} is obtained from the relation by Spitzer & Hart (1971)

$$t_{rlx} = \frac{8.9 \times 10^5 \sqrt{N} \times R_h^{3/2}}{\log(0.4N) \times \sqrt{m}} \quad (4)$$

where m and N refer to the mean mass and the number of the cluster members, respectively, taken from Col. 1 of Table 9. R_h is defined as the radius from the core that contains half the total mass of the cluster. This parameter has been inferred from Fig. 13, showing the cumulative mass in dependence of the radius. The half-mass radius (R_h) of NGC 1513 is 6'.16. For the conversion into pc, we considered 0.439 value (Col. 2 of Table 7). As an indicator of the dynamical evolution, the evolutionary parameter is estimated from the relation $\tau = Age/t_{rlx}$ by using its age (Gaia DR3) (Col. 5 of Table 6). Its Jacobi tidal radius R_J is estimated from the equation given by Portegies Zwart et al. (2010),

$$R_J = \left(\frac{GM}{2\omega^2} \right)^{1/3} \quad \omega = \frac{V_c}{R_{GC}} \quad (5)$$

where ω , M , V_c , R_{GC} are orbital angular frequency in the galaxy, the observed total mass (Col. 1 of Table 9), circular velocity (row 5 of Table 8), galactocentric distance (row 12 of Table 8), respectively. The concentration parameter is estimated from the relation $c = \log(R_t/R_{core})$. See sect.6.1 of Karataş et al. (2023) for the role of dynamical indicators in understanding of the dynamical evolution of the OCs. All the obtained dynamical parameters are given in Cols. 2-3 of Table 9.

The birth radius (R_{birth}) of NGC 1513 is estimated with the help of the current metallicity gradient based on young OCs, the model by Minchev et al. (2018) for the time evolution of the Galactic Interstellar Medium (ISM) metallicity gradient, its metal abundance (-0.06 dex) and age (Gaia DR3) (Table 6). Its guiding radius and migration distance are obtained from the relations $R_{guide} = J_z/V_\Phi$ and $d_{mig} = R_{guide} - R_{birth}$, respectively. The obtained parameters are listed in the last line of Table 9.

Table 9. The obtained parameters of mass information, dynamical parameters/dynamical indicators, and migration parameters for NGC 1513.

Mass information		Dynamical parameters		Dynamical indicators		Migration parameters	
Mass range (M_{\odot})	1.12 – 3.98	R_h (pc)	2.39 ± 0.26	c	0.74	R_{guide} (kpc)	9.57
MF slope (χ)	2.39 ± 0.25	R_J (pc)	19.88	R_{core}/R_h	0.82	R_{birth} (kpc)	9.11
Total mass (M_{\odot})	624.7 ± 7.4	t_{rlx} (Myr)	22.3 ± 5.9	R_h/R_t	0.22	d_{mig} (kpc)	0.46
Mean Mass (M_{\odot})	1.37 ± 0.06	t_{diss} (Myr)	421 ± 89	R_h/R_J	0.12		
Members (N)	457 ± 21	τ	11 ± 4	R_t/R_J	0.54		

Table 10. Literature comparison. Our results in row 1 are given for only $(B - V)$ colour index. The reddenings of different photometries are also listed in parentheses.

$E(B-V)$	$(V - M)_0$	d (pc)	Z	[Fe/H]	Age (Myr)	Isochrone	Photometry	Reference
NGC 1513								
0.79 ± 0.09	10.90 ± 0.15	1514 ± 105	0.013	-0.06	224 ± 27	Paxton et al. (2011)	CCD UBVR	This paper
0.65 ± 0.03	10.58 ± 0.16	1330 ± 100	0.019	–	225 ± 25	Girardi et al. (2000)	CCD UBVR	1
0.74 ± 0.06 ($E(J - H) = 0.23$)	11.53 ± 0.24	1180 ± 150	0.019	–	100 ± 20	Marigo et al. (2008)	JHK _S	2
0.67	10.95	1400	0.019	–	316	Marigo et al. (2008)	JHK _S	3
0.76 ± 0.16	10.60 ± 1.08	1320 ± 700	solar	–	251	Bertelli et al. (1994)	CCD BV	4
0.67	10.60 ± 0.00	1320	0.019	–	254	Girardi et al. (2000)	CCD BV	5
0.70 ($E(G - R) = 0.93$)	13.10	1323 ± 100	solar	–	150	ZAMS- SK1965	photographic RGU	6
0.52 ($A_V = 1.60$)	10.95	1546	solar	–	290	Bressan et al. (2012)	Gaia DR2	7

- 1 Sagar, R. et al., 2022, J. Astrophys. Astr.
- 2 Gunes, O. et al., 2017, AN, 338, 464
- 3 Kharchenko N.V. et al., 2013, A&A, 558, 53
- 4 Maciejewski, G. and Niedzielski, A., 2007, A&A, 467, 106

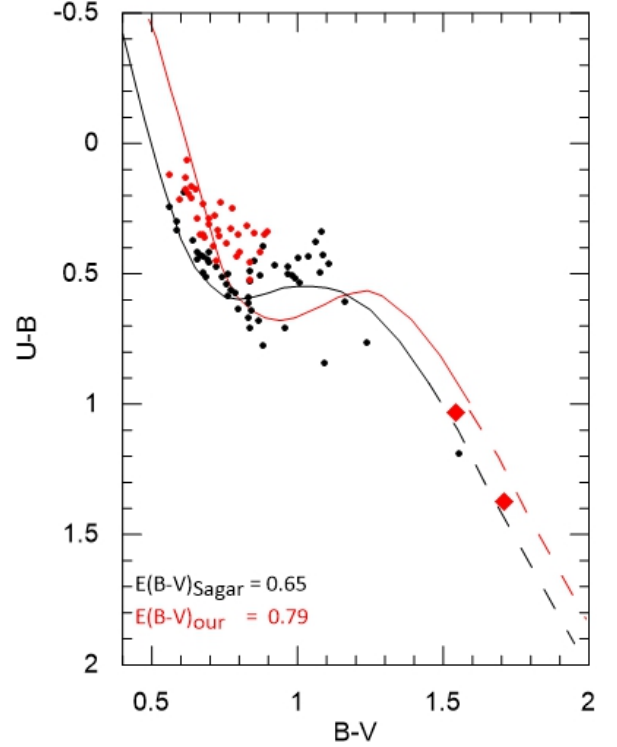
- 5 Frolov, V.N. et al., 2002, A&A, 396, 125
- 6 del Rio G., Huestamendia G. 1988, A&AS, 73, 425
- 7 Cantat-Gaudin, T. et al., 2020, A&A, 640, 1

11 DISCUSSION AND CONCLUSION

Within the error limits our $E(B - V) = 0.79 \pm 0.09$ mag is in concordance with the literature (Table 10). The discrepancies in the reddenings are quite small, $\Delta E(B - V) = 0.03$ to $+0.14$, except for the value 0.52 of Cantat-Gaudin et al. (2020). Our distance value (1514 ± 105) pc (Col. 3) is good agreement with the ones of 1471 ± 15 pc (Table 3, Gaia DR3 parallax) and 1546 pc of Cantat-Gaudin et al. (2020) (Table 10) within the uncertainties. Note that the previous literature provides close distances. The differences for distance are up to level, $\Delta d(\text{pc}) = 32$ to 334 pc.

With the age 224 ± 27 Myr ($\log \text{Age} = 8.35 \pm 0.05$), NGC 1513 is an intermediate age OC, according to the age interval 100–700 Myr ($7.0 \leq \log \text{Age} < 8.85$) given by S13. del Rio & Huestamendia (1988) and Güneş et al. (2017) give a relatively young age up to ~ 70 –120 Myr in terms of our age value. The age given by Kharchenko et al. (2013) is somewhat older than our detect. Our age value falls in the age interval of the rest literature with the uncertainties. The discrepancies of the age are at the level of 65 to 151 Myr.

The obtained ages from both this study (Table 10) and S22 are good agreement, although the different isochrones are used. For the isochrone selection, this study uses $Z = +0.013$ value, whereas S22 consider the solar abundance value, $Z = +0.019$. However, S22 give a somewhat low reddening $E(B - V) = 0.65$ mag and a close distance. This can be explained that our $(U - B)$ colours are bluer than the ones of S22 (Fig. 4c). In addition to this, as is seen from Fig. 14, the CC plot of S22 includes some early spectral-type stars as well as a few scattered FG-type stars around the bump. However, the CC plot of this study is occupied by early spectral type stars. S22 apply Schmidt-Kaler (Schmidt-Kaler 1982) ZAMS fit to their observations by assuming $R_V = 3.1$. Our $E(B - V)$ and R_V determination is based on the Q method for early type members and usage of S13 main-sequence.


Figure 14. The comparison of the CC diagrams of NGC 1513 for our (filled red dots) and S22 (filled black dots). The curves show the reddened S13 (red) and SK82 (black) main sequences. Red diamonds denote the bright evolved giants.

The small/large discrepancies in ages and distance moduli/distances (Table 10) stem from the adopted isochrones in terms of solar abundance, the reddening values from the CMDs or CCs, as well as different reduction techniques, as emphasized by Karataş et al. (2023).

The dynamic evolution of NGC 1513 has been interpreted with the help of dynamical parameters of the literature (Figs. 15-16). The values of $2000 M_{\odot}$ and $(R_{core}, R_{RDP}) = (1.5, 7)$ pc given by G17 are considered to classify the OCs as less massive/massive and large/small sized. With the $(R_{core}, R_{RDP}) = (1.96, 4.94)$ pc (panel a), NGC 1513 follows the increasing trend between R_{core} and R_{RDP} of Camargo et al. (2009) and G17. T22 state that R_{core} values of old age OCs are on average smaller than young ones. Internal dynamics can shape clusters cores after 100 Myr, while the shapes of young OCs originate from the initial conditions of the cluster formation. Our $R_{core} = 1.96$ pc value also falls in 1-2.5 pc interval in fig.7 of T22. In this context its relatively large R_{core} and small R_{RDP} may be due to its initial formation from molecular cloud.

Its age (224 Myr) is higher than its relaxation time (t_{rlx}) (Table 9). Therefore, it is dynamically relaxed. With its overall steep MFs ($\chi = +2.39$) and low $\tau = 10$, NGC 1513 falls in the range of $0.50 < \chi < 2.5$ in the χ versus τ , given by G17 (See their fig.27a). For the OCs with $\tau > 30$, their χ values tend to be negative because of the loss of low-mass stars, whereas their MFs show a flattening for the $\tau < 30$. This does necessarily mean that NGC 1513 presents a sign of small scale mass segregation with little dynamical evolution. Large scale mass segregation means that all stars in an OC have completed mass segregation, and thus the OC loses its low-mass content to the field. In the sense NGC 1513 did not lost much its low-mass stars to the field, owing to the internal/external perturbations. Its low mass stars outnumber its high mass stars, according to its MFs. Time scale parameters (t_{rlx}, τ) = (176 Myr, 0.57) of G17 also support the small mass segregation.

NGC 1513 presents multiple levels of mass segregation (Fig. 12). Λ_{MSR} drops to unity for around $N_{MST} = 190$. Therefore, almost 190 most massive stars with $\Lambda_{MSR} > 1$ are mass segregated. Beyond this limit, no any sign of mass segregation is seen. Accordingly, NGC 1513 ($\log Age = 8.35$) falls in the interval of $\log Age$ distribution with mass-segregation of T22 (See their fig.14).

The position of NGC 1513 in the R1 and R3 regions (Figs. 15b-c) does not indicate signs of expansion and shrinkage. The relationship between the cluster dimensions and age is linked to survival and dissociation rates of the OCs (Camargo et al. 2009). NGC 1513 resides in the second quadrant ($\ell = 152^{\circ}.59$) and $R_{GC} = 9.57$ kpc (outside the solar circle) together with its relatively small mass ($\sim 625 M_{\odot}$).

The relations among the internal and external dynamical evolution parameters (Table 9) for NGC 1513 (black dot) are shown in the panels of Fig. 16 together with the data of A20-21 (gray dots). Within the error limits NGC 1513 is almost close to the general trends in the panels. From panel (a), its relatively large R_{core} indicate that it is dynamically evolved ($\log \tau = 1.04$). Its $R_h = 2.34$ pc is greater than its $R_{core} = 1.96$ pc, and thus it meets the requirement of compliance with the general trend (panel c).

NGC 1513 with a high $R_{core}/R_h = 0.82$ and a compact $R_h/R_t = 0.22$ deviates from the trend in panel (d). Note that R_h detection between this study (Fig. 16) and A20/A21 is different, and their R_h is based on the relation $R_h = 1.3 a$ by using Plummer's a parameter (Plummer 1911) from the RDP profile fit.

Its relatively high R_{core}/R_h ratio is probably related to cluster-formation effects due to its little dynamical evolution, instead of exposing to two-body relaxation and mass segregation in its core region.

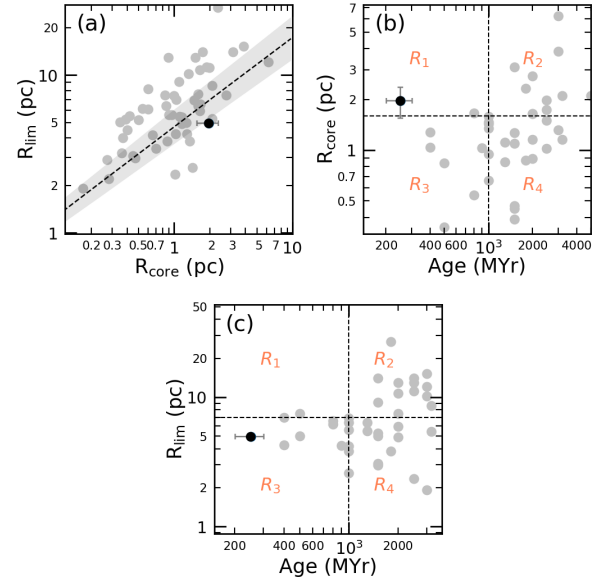


Figure 15. R_{RDP} versus R_{core} (panel a), (R_{core}, R_{RDP}) versus Age (panels b-c). The relation (dotted line) and its 1σ uncertainty as the shaded area in panel (a), the regions R1 – R4 in panels (b)-(c), the horizontal/vertical dotted lines to separate small/large sized OCs, and the comparison OCs (gray dots) are from G17.

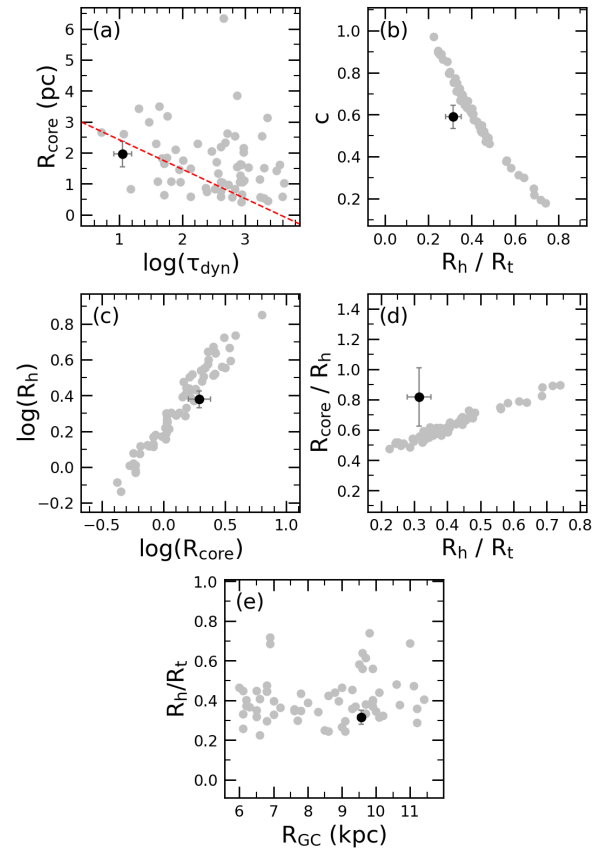


Figure 16. R_{core} versus $\log(\tau)$ (panel a), c versus R_h/R_t (panel b), $\log(R_h)$ versus $\log(R_{core})$ (panel c), R_{core}/R_h versus R_h/R_t (panel d), R_h/R_t versus R_{GC} (panel e). The gray filled dots in the panels and the dashed line (panel a) are from A20 and A21. The position of NGC 1513 in the panels is shown with the black dot.

Based on the simulations of Heggie & Hut (2003), the R_{core}/R_h tends to decrease as the cluster dynamically evolves, since internal relaxation combined with the preferential evaporation of lower-mass regulated by the external potential, leads to a higher degree of central concentration. Since NGC 1513's central structure with the high R_{core}/R_h ratio occupies a considerably high fraction of the cluster main structure, despite the fact that it is little dynamically evolved OC ($\tau = 10$), this inflated central structure may be consequence of the formation process. Without the firm arguments based on the simulations, we avoid the possibility of rapid expulsion.

The concentration parameter (c) gives some evidence regarding the OC dynamical state. Its $c = 0.74$ (panel b), small $R_h/R_t = 0.22$ and $R_h/R_j = 0.12$ ratios imply that NGC 1513 is a compact OC. R_h/R_t is also as an indicator of the tidal influence of the Galaxy on the dynamical evolution of the OCs. its R_h/R_t is smaller than the tidally limit, $R_h/R_t = 0.40$ given by Heggie & Hut (2003). According to these compact ratios, its dynamical evolution is driven by its internal relaxation. Its low R_h/R_j ratio also falls in the range of 0.10-0.23 according to figure 2 of Heggie & Hut (2003). This value is also smaller than $R_h/R_j = 0.35$, given by A23. This points out that it is a tidally filled OC.

When the all evidences of no any signs of expansion/shrinkage (Fig. 15b-c), a high R_{core}/R_h , compact R_h/R_t and R_h/R_j ratios are evaluated together as the dynamic indicators, NGC 1513 exposes less to the tidal stripping/disruption of the external perturbations without being tidally disrupted. These external perturbations are the collisions with massive GMCs, tidal effects from spiral arms, disc and Bulge crossings. Its distant location $R_{GC} = 9.57$ kpc has also an advantage in preserving stellar content against these external perturbations.

As emphasized in the paper of Karataş et al. (2023), a tidal radius much larger than the Jacobi radius ($R_t/R_j \geq 1$) might be linked to significant mass loss due to tidal effects. R_t/R_j is the Roche volume filling factor, as the tidal to Jacobi radius ratio. A23 state that the OCs with $R_t/R_j \geq 1.25$ are tidally overfilled. The OCs with $R_t/R_j < 1$ keep their stellar content within its Jacobi radius. In light of this information, its Roche lobe is gravitationally bound to the cluster, and thus NGC 1513 with $R_t/R_j = 0.54$ appears to keep its stellar content with the advantage of exposing less to the tidal effects due to its distant position plus its one revolution around the center of the galaxy. $R_j = 20.20$ pc value given by Hunt & Reffert (2024) supports this conclusion, which is in compatible with our $R_j = 19.88$ pc value (Col. 2 of Table 9). In summary, for NGC 1513, mass segregation and two body relaxation as internal dynamical evolution seem to be efficient than cluster evaporation process.

We find that NGC 1513 migrated about 0.46 kpc from its birth place. It has guiding radius fairly near its birth radius. Its least migration rate is also compatible with the cluster's low evaporation due to low-mass loss and little dynamical evolution (small τ).

ACKNOWLEDGMENTS

We thank Dr. M. Netopil for providing us the metal abundance value from his DG method, and for the valuable discussion on the analysis. R. Sagar is also thanked for providing CCD *UBV* data of NGC 1513 for the comparison. We also thank Drs. O. Gunes and M. Angelo for valuable comments on the dynamical evolution. The open cluster data is based upon observations carried out at the Observatorio Astronómico Nacional on the Sierra San Pedro Mártir (OAN-SPM), Baja California, México. This paper has made use of results from the European Space Agency (ESA) space mission Gaia, the data

from which were processed by the Gaia Data Processing and Analysis Consortium (DPAC). Funding for the DPAC has been provided by national institutions, in particular the institutions participating in the Gaia Multilateral Agreement. The Gaia mission website is <http://www.cosmos.esa.int/gaia>. This paper has also made use of the WEBDA database, operated at Department of Theoretical Physics and Astrophysics of the Masaryk University, Brno (the Vienna site is just a backup). This publication also makes use of SIMBAD database-VizieR (<http://vizier.u-strasbg.fr/viz-bin/VizieR?-source=II/246>).

DATA AVAILABILITY

The photometric data of NGC 1513 can be requested from Raul Michel (rmm@astro.unam.mx).

REFERENCES

- Akkaya Í., Schuster W.J., Michel R., Chavarría-K C., Moitinho A., Vázquez R., Karataş Y., 2010, *Rev. Mex. Astron. Astrofis.*, 46, 385
- Akkaya Oralhan Í., Karataş Y., Schuster W.J., Michel R., Chavarría C., 2015, *New Astron.*, 34, 195
- Akkaya Oralhan I., Michel R., Schuster W.J., Karataş Y., Karşlı Y., Chavarría C., 2019, *J. Astrophys. Astron.*, 40, 33
- Allison, R.J., Goodwin, S.P., Parker, R.J., Portegies-Zwart, S.F., de Grijs, R., Kouwenhoven, M.B.N., 2009, *MNRAS*, 395, 1454
- Angelo M.S., Santos Jr J.F.C., Corradi W.J.B., 2020, *MNRAS*, 493, 3473
- Angelo M.S., Corradi W.J.B., Santos Jr J.F.C., Maia F.F.S., Ferreira F.A., 2021, *MNRAS*, 500, 4338
- Angelo M.S., Santos Jr J.F.C., Maia F.F.S., Corradi W.J.B., 2023, *MNRAS*, 522, 956
- Arenou F., Luri X., Babusiaux C., et al., 2018, *A&A* 616, 17
- Bailer-Jones C.A.L., Rybizki J., Fouesneau M., Mantelet G., Andrae R., 2018, *AJ*, 156, 58
- Balaguer-Nunez L., Tian K.P., Zhao J.L., 1998, *A&AS*, 133, 387
- Bertelli, G., Bressan, A., Chiosi, C., Fagotto, F., Nasi, E. 1994, *A&AS*, 106, 275
- Bessell M., 2005, *ARA&A*, 43, 293
- Bica E, Bonatto C., 2005, *A&AS*, 443, 465.
- Bland-Hawthorn J., Ortwin Gerhard O., 2016, *ARA&A*, 54, 529
- Bonatto C., Bica E., Santos Jr J.F.C., 2005, *A&A*, 433, 917
- Bonatto C., Bica E., 2007, *MNRAS*, 377, 1301
- Bonatto C, Bica E., 2009, *MNRAS*, 397, 1915.
- Bonatto C, Bica E., 2010, *A&A*, 521, 74.
- Bovy J., galpy: A python Library for Galactic Dynamics., 2015, *ApJS*, 216, 29
- Bragaglia, A., Fu, X., Mucciarelli, A., Andreuzzi, G., Donati, P. 2018, *A&A*, 619, 176
- Bressan A., Marigo P., Girardi L., Salasnich B., Dal Cero C., Rubele S., Nanni A., 2012, *MNRAS*, 427, 127
- Brunthaler A., Reid M.J., Menten K.M., et al., 2011, *Astron. Nachr*, 332, No.5, 461
- Bukowiecki L., Maciejewski G., Konorski P., Strobel A., 2011, *Acta Astron.*, 61, 231
- Buser R, 1978, *A&A*, 62, 411
- Cakmak H., Gunes O., Karatas Y., Bonatto C., 2021, *Astron. Nachr*, 324, 975
- Cakmak H., Karatas Y., 2022, *New Astronomy*, 960, 1833
- Camargo D., Bonatto C., Bica E., 2009, *A&A*, 508, 211
- Carney, B., 2001, *Star Clusters*, Saas-Fee Advanced Course 28, Lecture Notes 1998, Swiss Society for Astrophysics and Astronomy, eds. L. Labhardt and B. Binggeli (Berlin: Springer-Verlag) p.1-222
- Cantat-Gaudin T., Anders F., Castro-Ginard A., et al., 2020, *A&A*, 640, 1
- Choi J., Dotter A., Conroy, C. et al. 2016, *ApJ*, 823, 102
- del Rio, G., Huestamendia, G., 1988, *A&AS*, 73, 425
- Dean J.F., Warren P.R., Cousins A.W.J., 1978, *MNRAS*, 183, 569

- Dias W.S., Monteiro H., Lepine J.R.D., prates R., Gneiding C.D., Sacchi M. 2018, MNRAS, 481, 3887
- Dotter A. 2016, ApJS, 222, 8
- Fernie, J.D., 1963, AJ, 68, 780.
- Fitzpatrick, E. L., & Massa, D. 2009, ApJ, 699, 1209
- Frolov, V.N., Jilinski, E.G., Ananjevskaia, J.K. et al., 2002, A&A396, 125, 130
- Gaia Collaboration Vallenari, A., Brown, A. G. A., et al., 2023, A&A, 674, A1
- Gaia Collaboration Montegriffo, P., Bellazzini, M., De Angeli, F., et al., 2023, A&A, 674, A33
- Gieles M., Athanassoula E., Portegies-Zwart S., 2007, MNRAS, 376, 809
- Girardi L., Bressan A., Bertelli G., Chiosi C., 2000, A&AS, 141, 371
- Girardi L., Bertelli G., Bressan A., Chiosi C., Groenewegen M.A.T., Marigo P., Salasnich B., Weiss A., 2002, A&A, 391, 195
- Groenewegen M. A. T., 2021, A&A, 654, A20
- Guetter, H. H., & Vrba, F. J. 1989, AJ, 98, 611
- Güneş, O., Karataş, Y., Bonatto C., 2017, Astronomische Nachrichten (AN), 338, 464.
- Heggie D. and Hut P., 2003, the gravitational million-body problem: A multidisciplinary approach to star cluster dynamics, Cambridge Univ. Press, chapter 33.
- Hunt, E.L. and Reffert, S., 2024, A&A, 2024arXiv240305143
- Johnson D.R.H., Soderblom D.R., 1987, AJ, 93, 864
- Karataş, Y., Cakmak, H., Akkaya-Oralhan, İ., et al., 2023, MNRAS, 521, 2408
- Kharchenko N.V., Piskunov A.E., Schilbach E., Röser S., Scholz R.D., 2013, A&A, 558, 53
- King I., 1962, AJ, 67, 471
- King I., 1966, AJ, 71, 64
- Kroupa P., 2001, MNRAS, 322, 231.
- Lamers H.J.G.L.M., Gieles M., 2006, A&A, 455, 17
- Landolt, A.U., 1973, AJ, 78, 959
- Landolt, A.U., 1983, AJ, 88, 439
- Landolt A.U., 2009, AJ, 137, 4186
- Lim, B., Sung, H., Kim, J.S., Bessell, M., Park, B-G., 2014, MNRAS, 443, 454
- Lim, B., Rauw, G., Nazé, Y., Sung, H., Hwang, N., Park, B-G., 2019, NatAs, 3, 76
- Maciejewski, G. and Niedzielski, A., 2007, A&A, 467, 1065
- Marigo, P., Girardi, L., Bressan, A., Groenewegen, M. A. T., Silva, L., & Granato, G. L., 2008, A&A, 482, 883 (M08)
- Minchev I., Anders F., Recio-Blanco A., et al. 2018, MNRAS, 481, 1645
- Netopil, M., Paunzen, E., 2013, A&A, 557, A10
- Netopil M., Paunzen E., Carraro G., 2015, A&A, 582, A19
- Netopil M., Paunzen E., Heiter U., Soubiran C., 2016, A&A, 585, A150
- Netopil M., Oralhan- Akkaya, İ., Cakmak H., Michel R., Karatas Y. 2022, MNRAS, 509, 421
- Paxton, B., Bildsten, L., Dotter, A. et al., 2011, ApJS, 192, 3
- Paxton, B., Cantiello, M., Arras, P., 2013, ApJS, 208, 4
- Paxton, B., Marchant, P., Schwab, J., et al., 2015, ApJS, 220, 15
- Paxton, B., Schwab, J., Bauer, E. B., et al. 2018, ApJS, 234, 34
- Paxton, B., Smolec, R., Schwab, J., et al. 2019, ApJS, 243, 10
- Pedregosa F., et al., 2011, Journal of Machine Learning Research, 12, 2825.
- Piatti A.E., Dias W.S., Sampedro L.M., 2017a, MNRAS, 466, 392
- Piatti A.E., 2017b, MNRAS, 465, 2748
- Piatti A.E., Angelo M.S., Dias W., 2019, MNRAS, 488, 4648
- Plummer, H.C., 1911, MNRAS, 71, 460
- Pöhl H., Paunzen E., 2010, A&A, 514, A81
- Simon F. Portegies Zwart, S.F., McMillan, S.L.W., and Mark Gieles, M., 2010, ARA&A, 48, 431
- Sagar R., Yadav, R.K.S., Pandey, S.B., J. Astrophys. Astr., 43, 31
- Sariya D.P., Yadav R.K.S., Yadav Bellini A., 2012, A&A, 543, 87
- Schilbach, E., Kharchenko, N. V., Piskunov, A. E., Röser, S., & Scholz, R. D. 2006, A&A, 456, 523
- Schönrich R., Binney J., Dehnen W., 2010, MNRAS403, 1829
- Schmidt-Kaler, Th. 1982, in Landolt-Bornstein, Numerical Data and Functional Relationships in Science and Technology, New Series, Group VI, Vol.2b, eds. K. Schaifers & H. H. Voigt (Berlin: Springer), p. 14 (SK82)
- Schuster W.J., Michel R., Dias W., Tapia-Peralta T., Vázquez R., Macfarland J., Chavarría C., Santos C., Moitinho A., 2007, Galaxy Evolution Across the Hubble Time, eds. F. Combes and J. Palouš, Proceedings of the International Astronomical Union, IAU Symposium No. 235, (Cambridge, United Kingdom: Cambridge University Press), p. 331
- Skrutskie M.F., Cutri R., Stiening R., Weinberg M.D., Schneider S.E., Carpenter J.M., Beichman C., Capps R., 2006, AJ, 131, 1163
- Soubiran C., 2018, A&A, 619, 155
- Soubiran C., et al., 2019, A&A, 623, 2
- Spitzer L., Hart M. ,1971, AJ, 164, 399
- Stetson P.B., 1987, PASP, 99, 191
- Straizys V., 1995, Multicolor Stellar Photometry, Astronomy and Astrophysics Series, Vol. 15, ed. A.G. Pacholczyk (Tucson, Arizona: Pachart Pub. House)
- Sung, H. and Bessell, M.S., 2000, PASA, 17, 244
- Sung, H., Lim, B., Bessell, M.S. Kim, J.S., Hur, H., Chun, M-Y., Park, B-G., 2013, JKAS, 46, 97
- Sung, H., and Bessell, M. S., 2014, ASP Conference Series, Vol. 482..p.275-277, ed. Hee-Won Lee, Young Woon Kang, and Kam-Ching Leung. San Francisco, CA: Astronomical Society of the Pacific
- Tapia M. T., Schuster W. J., Michel R., Chavarría-K C., Dias W. S., Vázquez R., & Moitinho A., 2010, MNRAS, 401, 621
- Tarriq Y., Soubiran C., Casamiquela L., Castro-Ginard A., Olivares J., Miret-Roig N., Galli P.A.B., 2022, A&A, 659, A59
- Wu Z.Y., Tian K.P., Balaguer-Nunez L., Jordi C., Zhao J.L., and Guibert J., 2002, A&A, 381, 464